CrossMark

Clues to the Formation of Liller 1 from Modeling Its Complex Star Formation History

Emanuele Dalessandro[1] , Chiara Crociati[1,2], Michele Cignoni[1,3,4] , Francesco R. Ferraro[1,2] , Barbara Lanzoni[1,2] ,
Livia Origlia[1] , Cristina Pallanca[1,2] , R. Michael Rich[5], Sara Saracino[6] , and Elena Valenti[7,8]

[1] Istituto Nazionale di Astrofisica (INAF), Osservatorio di Astrofisica e Scienza dello Spazio di Bologna, Via Gobetti 93/3, I-40129 Bologna, Italy
emanuele.dalessandro@inaf.it

[2] Dipartimento di Fisica e Astronomia, Universitá di Bologna, Via Gobetti 93/2, I-40129 Bologna, Italy
[3] Department of Physics, University of Pisa, Largo Pontecorvo, 3, I-56127 Pisa, Italy
[4] INFN, Largo B. Pontecorvo 3, I-56127 Pisa, Italy
[5] Department of Physics and Astronomy, University of California, Los Angeles, Los Angeles, CA, USA
[6] Astrophysics Research Institute, Liverpool John Moores University, Liverpool, UK
[7] European Southern Observatory, Garching, Germany
[8] Excellence Cluster ORIGINS, Garching, Germany

Abstract

Liller 1 and Terzan 5 are two massive systems in the Milky Way bulge hosting populations characterized by significantly different ages ($\Delta t > 7$–8 Gyr) and metallicities (Δ[Fe/H] ~ 1 dex). Their origin is still strongly debated in the literature and all formation scenarios proposed so far require some level of fine-tuning. The detailed star formation histories of these systems may represent an important piece of information to assess their origin. Here we present the first attempt to perform such an analysis for Liller 1. The first key result we find is that Liller 1 has been forming stars over its entire lifetime. More specifically, three broad star formation episodes are clearly detected: (1) a dominant one, occurring some 12–13 Gyr ago with a tail extending for up to $\sim$3 Gyr; (2) an intermediate burst, between 6 and 9 Gyr ago; and (3) a recent one, occurring between 1 and 3 Gyr ago. The old population contributes to about 70% of the total stellar mass, and the remaining fraction is almost equally split between the intermediate and young populations. If we take these results at face value, they would suggest that this system unlikely formed through the merger between an old globular cluster and a giant molecular cloud, as recently proposed. On the contrary, our findings provide further support to the idea that Liller 1 is the surviving relic of a massive primordial structure that contributed to the Galactic bulge formation, similarly to the giant clumps observed in star-forming high-redshift galaxies.

1. Introduction

Among the vast population of Galactic stellar aggregates traditionally classified as globular clusters (GCs), three systems, namely Terzan 5, Liller 1, and ω Centauri, stand out for their significantly peculiar properties. With masses larger than some $10^6 M_\odot$, these objects are among the most massive cluster-like systems in the Galaxy. More importantly, they are the only ones hosting multiple populations characterized by both significant iron and age spreads ($\sim$1 dex and up to 5–8 Gyr, respectively; e.g., Norris et al. 1996; Lee et al. 1999; Pancino et al. 2000; Ferraro et al. 2009; Ferraro et al. 2021).

ω Centauri is a metal-poor (average metallicity $< $[Fe/H]$> \sim -1.5$) system orbiting the Galactic halo and hosting at least 4–5 discrete populations, as revealed by a large number of detailed photometric and spectroscopic analyses (e.g., Norris et al. 1996; Lee et al. 1999; Pancino et al. 2000; Ferraro et al. 2004; Sollima et al. 2005; Bellini et al. 2009; Johnson 2010). These populations span a wide metallicity range, going from [Fe/H] ~ -2.2 dex to -0.5 dex, and a possible age range of about 3–4 Gyr. This evidence led to the early suggestion that ω Centauri is the remnant core of an accreted dwarf galaxy captured during its approach to the Milky Way (Zinnecker et al. 1988;

Majewski 2000). Indeed, more recently, thanks to the exquisite Gaia astrometry (Gaia Collaboration et al. 2021), ω Centauri has been associated with either Gaia–Enceladus or Sequoia (Massari & Koppelman 2019), which are two of the most prominent accretion events experienced by the galaxy.

On the contrary, both Terzan 5 and Liller 1 are suspected to be the result of a different and very peculiar formation process. Terzan 5, for which detailed high-resolution photometric and spectroscopic analyses have been performed (Ferraro et al. 2009; Origlia & Rich 2011; Massari et al. 2014), hosts at least three subpopulations: (i) a dominant old population that formed about 12 Gyr ago from gas enriched by Type II supernovae (SNe), with subsolar metallicity ([Fe/H] $= -0.3$) and enhanced [α/Fe] abundance ratio; (ii) a younger population formed about 4.5 Gyr ago, from gas characterized by supersolar metallicity ([Fe/H] $= +0.3$) and solar-scaled [α/Fe]; and (iii) an additional metal-poor [Fe/H] $= -0.7$ and enhanced [α/Fe] abundance ratio. The [α/Fe]–[Fe/H] pattern of Terzan 5 is strikingly similar to that of bulge stars (Ness et al. 2013; Johnson et al. 2013; Gonzalez et al. 2015; Rojas-Arriagada et al. 2017; Queiroz et al. 2020), and totally incompatible with what was observed in the Milky Way outer disk and halo and in local dwarf galaxies. In addition, the reconstructed orbit indicates that Terzan 5 always remained well confined within the bulge (Massari et al. 2015). All these facts strongly disfavor the possibility that Terzan 5 formed in a satellite galaxy later accreted by the Milky Way, and rather suggest that it is a genuine Galactic system, which formed

and evolved in and with the bulge. More recently, Ferraro et al. (2021) discovered the presence of at least two distinct subpopulations with remarkably different ages also in Liller 1. One population has an age of 12 Gyr, and the other one possibly is as young as 1 Gyr. The oldest populations in Liller 1 and Terzan 5 are impressively similar, in agreement with the typical age of bulge GCs and most of bulge stars. This indicates strikingly that they both formed at the same cosmic epoch, thus likely from gas clouds with compatible chemistry. Indeed, the metallicity of the few giant stars investigated so far in Liller 1 is perfectly compatible with that of the old population in Terzan 5: [Fe/H] ~ -0.3 and [α/Fe] $\sim +0.3$ (Origlia & Rich 2002). An in situ origin, instead of an accretion from outside, therefore seems to be plausible also for Liller 1.

Ferraro et al. (2009) and Ferraro et al. (2021) suggested that these stellar systems could be interpreted as the surviving relics of much more massive primordial structures that generated or contributed to the Galactic bulge formation, similarly to the giant clumps observed in the star-forming regions of high-redshift galaxies (Immeli et al. 2004; Carollo et al. 2007; Elmegreen et al. 2008; Genzel et al. 2011; Tacchella & Carollo 2015; Behrendt et al. 2016). In fact, observations of high-z spiral galaxies often show bright UV clumps within them (Cowie et al. 1995; van den Bergh et al. 1996; Giavalisco & Steidel 1996; Elmegreen et al. 2004, 2005; Shibuya et al. 2016), indicative of massive star-forming complexes. Although many of these clumps are expected to migrate to the center of the host galaxy, due to dynamical friction, and deposit their stars there, effectively building the bulge of these protogalaxies (Immeli et al. 2004; Dekel et al. 2009), it is possible that a few of them survived the total disruption, producing stellar systems grossly appearing like massive stellar clusters (Bournaud 2016). These fossil relics could have been extremely massive in the past thus being able to retain the iron-enriched ejecta of SNe explosions, possibly producing the subpopulations now observed in Terzan 5 and Liller 1.

Terzan 5 and Liller 1 would therefore belong to a new class of stellar systems called (Ferraro et al. 2021) bulge fossil fragments: these are stellar aggregates with the appearance of massive GCs orbiting the Galactic bulge, formed at the epoch of the galaxy assembling, and harboring, in addition to the old population, a younger component.

An alternative formation scenario for Terzan 5 and Liller 1 has been recently proposed by Bastian & Pfeffer (2022). The authors argue that their peculiar properties might be the result of an interaction between an ancient massive stellar cluster and a giant molecular cloud (GMC) that took place a few Gyr ago, thus forming the younger population observed in both systems. Based on the hydrodynamical simulations by McKenzie & Bekki (2018), they suggest that, as a result of such interaction, the massive cluster may be able to accrete gas from the GMC and eventually experience a new event of star formation. In this scenario, the probability of encounters between clusters and GMCs increases for massive systems on disky orbits, as in the case of Liller 1 and Terzan 5, but in general it remains pretty low. As these are rare events, only an handful of systems is expected to undergo this formation process within a Hubble time. In addition, because of their rarity, stellar systems forming this way are expected to produce two discrete star formation episodes. In this scenario, the metal-poor ([Fe/H] $= -0.7$) subpopulation of Terzan 5 is composed by captured field stars.

In this ongoing and exciting discussion about the physical processes behind the formation of Terzan 5 and Liller 1, constraining the detailed star formation histories (SFHs) of their stellar populations represents an important piece of information. Driven by this motivation, in this paper we perform the very first attempt to reconstruct the SFH of these complex stellar systems by using Liller 1 as a test-bench. In fact, the available photometric data set for Liller 1 has a larger photometric completeness, and the main-sequence turn-off of the younger population is brighter than in Terzan 5.

The paper is structured as follows. Section 2 presents the available data sets adopted for this study and it describes the main steps of the data analysis. In Section 3 we describe the relative proper motion analysis to separate likely cluster members from field interlopers, and in Section 4 we briefly describe the artificial star experiment construction. Section 5 briefly describes the approach used to reconstruct the SFH of Liller 1 and reports on the main results. In Section 6 we summarize our findings and discuss them in the context of the formation scenarios for this system.

2. Observations and Data Analysis

The photometric data set used in this study combines optical and IR high-resolution images. The optical database includes images acquired with the Hubble Space Telescope (HST) Advanced Camera for Survey/Wide Field Channel (ACS/WFC) through proposal GO 15231 doi:10.17909/7zah-te68 (PI: Ferraro). It consists of 12 deep images obtained with the filters F606W (6 images with exposure time $t_{exp} = 1300$ sec) and F814W (6 images with $t_{exp} = 600$). The ACS/WFC is composed of two twin chips, each of 4096×2051 pixels, separated by a gap of approximately 30 pixels. The pixel scale is $0\rlap{.}''05$ pixel^{-1}; therefore, the resulting field of view (FOV) is $204'' \times 204''$. As shown in Figure 1, the cluster is centered in chip 1. All images are dithered by a few pixels to allow a better subtraction of CCD defects, artifacts, and false detections, and eventually a better sampling of the stellar point-spread function (PSF).

The IR data set was obtained with the camera Gemini South Adaptive Optics Imager (GSAOI) assisted by the Gemini Multi-Conjugate Adaptive Optics System (GeMS) mounted at the 8 m Gemini South Telescope (Chile; Program ID: GS-2013-Q-23; PI: D. Geisler). GSAOI is equipped with a 2×2 mosaic of Rockwell HAWAII-2RG 2048×2048 pixels arrays with a resolution of 0.02 pixel^{-1} (Neichel et al. 2014). The central region of Liller 1 was sampled with a mosaic of multiple exposures acquired with a dithering pattern of a few arcseconds resulting in a global FOV of $95'' \times 95''$ on the sky (Figure 1). Specifically, a total of 7 and 10 exposures were acquired in three nights from 2013 April 20 to May 24 in the J and K_s bands, respectively, with $t_{exp} = 30$ s each. This data set was analyzed and presented by Saracino et al. (2015) in the first instance. Here we reanalyzed only the six best-quality images in terms of delivered FWHM, encircled energy, and Strehl ratio (see Dalessandro et al. 2016) for both the available filters.

The photometric reduction was carried out by performing PSF fitting in each chip of each image independently for both the IR and the optical data by using DAOPHOTIV (Stetson 1987). The PSF has been modeled by selecting about 200 bright and isolated stars uniformly distributed in each chip and by using the DAOPHOTIV/PSF routine. We allowed the PSF to vary within each chip following a cubic polynomial spatial
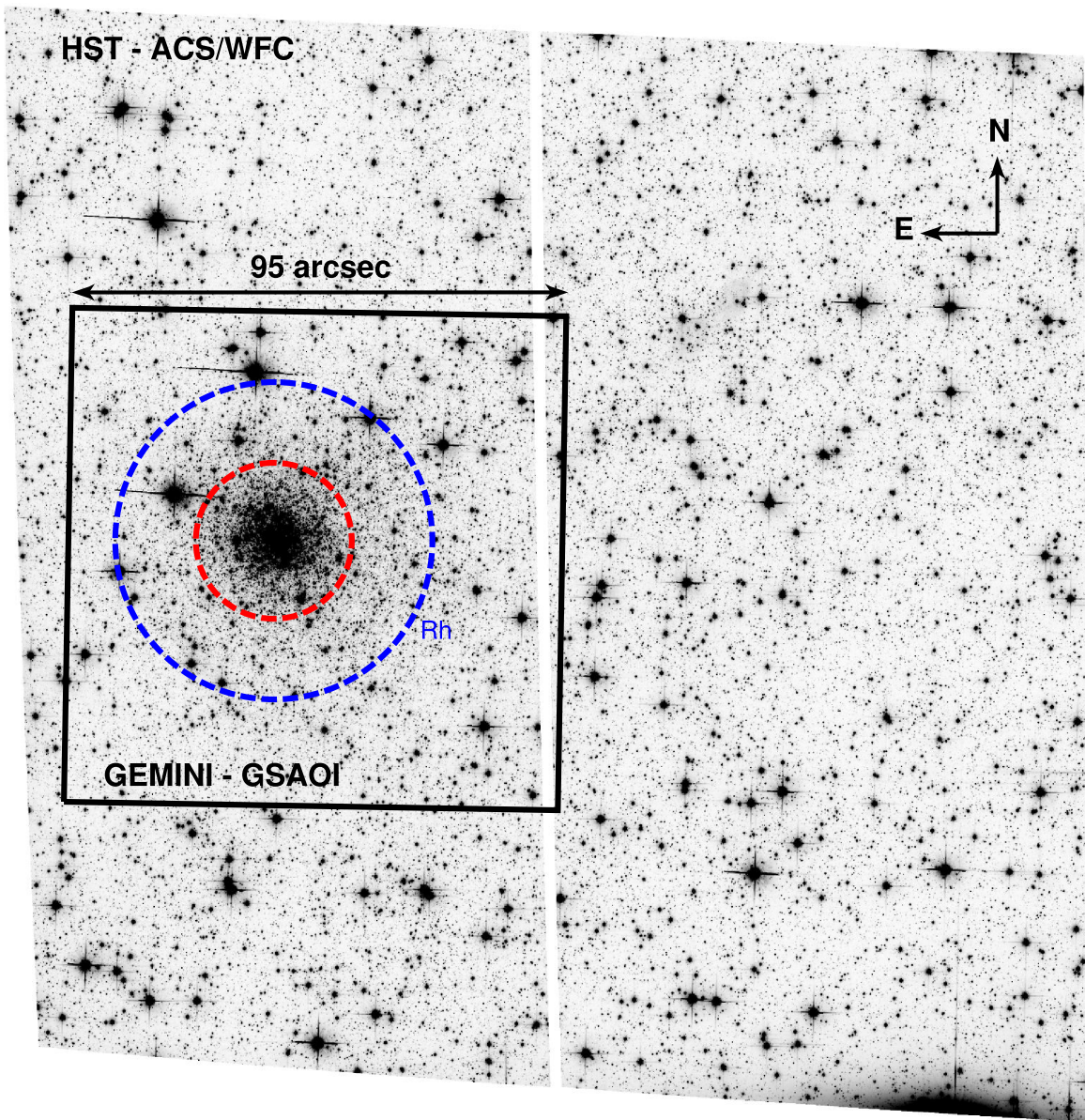
Figure 1. HST ACS/WFC image of Liller 1 in the F814W filter. The field of view is $204'' \times 204''$. The black box corresponds schematically to the GeMS-GSAOI pointing ($95'' \times 95''$). The region used for the SFH reconstruction is that beyond the red circle (having a radius of $15''$). The blue circle marks the half-mass–radius of Liller 1 ($r_h = 30''.5$; from Saracino et al. 2015). North is up; east is to the left.

variation. The PSF models thus obtained were then applied to the star-like sources detected at a 3σ level above the local background in all images by using ALLSTAR. We then created a master list including stars detected in at least three HST F814W (that will be labeled hereafter as I) and GeMS K_s (simply labeled as K) images. This choice was driven by the fact that both the F606W and J images are significantly shallower than the I and K ones because of the extremely high extinction ($E(B-V) = 4.52$; Ferraro et al. 2021) in the direction of Liller 1 and because of the reduced efficiency of the AO corrections in the J band. As done in previous works (e.g., Dalessandro et al. 2018 and references therein), the master list thus created was used as input for ALLFRAME (Stetson 1994) and, at the corresponding positions of stars in the master list, a fit was forced in each frame of the two data sets. For each star thus recovered, multiple magnitude estimates obtained in each chip were homogenized by using DAOMATCH

and DAOMASTER, and their weighted mean and standard deviation were finally adopted as star magnitude and photometric error. The obtained catalog includes 62,834 stars in total. Of them, 51,100 have both I and K magnitudes.

We reported the instrumental optical magnitudes onto the VEGAMAG photometric system by using the updated recipes and zero-points available in the HST websites.[9] To calibrate the IR magnitudes, we used the stars in common between GeMS and the VISTA Variables in the Vía Láctea (VVV) survey (Minniti & Lucas 2010). The calibration zero-points were then set as the difference between the J and K magnitudes in the two samples, after applying an iterative 3σ-clipping algorithm. The resulting ($I–K$, I) color–magnitude diagram (CMD), including the differential reddening corrections (DRCs) derived by Pallanca et al. (2021), is shown in Figure 2 (left panel).

---

[9] https://www.stsci.edu/hst/instrumentation/acs/data-analysis/zeropoints
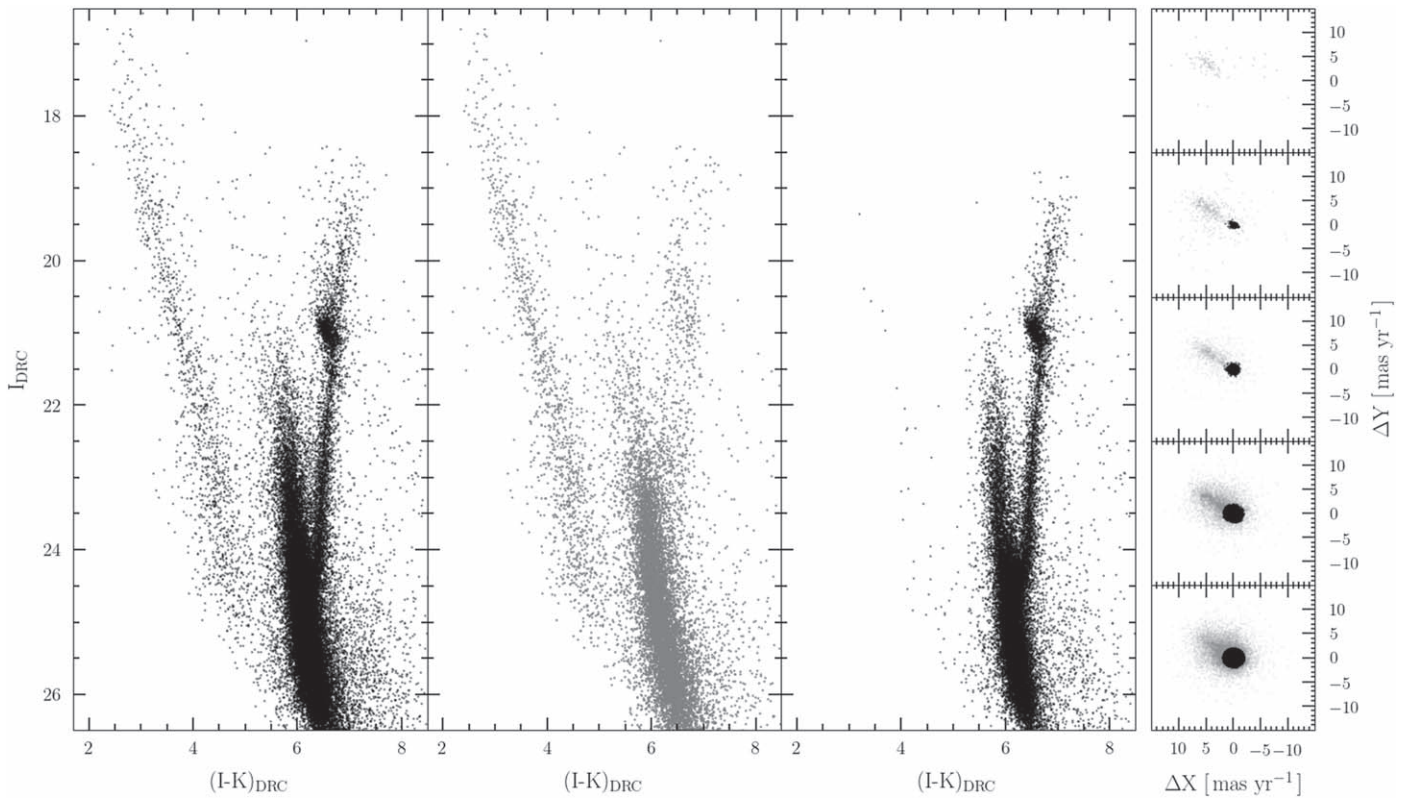
Figure 2. Panel (a): differential reddening-corrected (I, $I–K$) CMD of the stars in common between GEMINI and HST, and with measured PMs. Panel (b): CMD of the field population as selected from the VPDs as those with PMs not compatible with that of Liller 1. Panel (c): PM-cleaned CMD of Liller 1 obtained by using only the likely cluster members selected from the VPDs shown in the rightmost column. Rightmost column: VPDs of the measured stars divided in five bins of 2 mag each, starting at $I_{DRC} = 16.5$. Black dots represent the stars selected as likely cluster members (see Section 3).

Instrumental coordinates (x, y) were first reported to the HST ACS/WFC reference frame. Then they were corrected for geometric distortions by using prescriptions by Anderson & Bedin (2010) and Ubeda et al. (2012) and were then transformed to the absolute coordinate (α, δ) system by using stars in common with the publicly available early Gaia Data Release 3 (Gaia eDR3) catalog (Gaia Collaboration et al. 2021). About 200 stars have been matched by using the cross-correlation tool `CataXcorr`, thus allowing a very precise determination of the stellar absolute positions. We note in passing that almost all the stars in common with the Gaia catalog are disk field stars. The resulting 1σ astrometric accuracy is $\sim 0\rlap{.}''1$.

3. Proper Motion Analysis

Figure 2 shows that, as expected given its position in the galaxy, the evolutionary sequences of Liller 1 are quite strongly contaminated by a significant fraction of field stars. The blue sequence visible at $I_{DRC} < 25$ and $(I–K)_{DRC} < 5.5$ is very prominent and likely populated by young disk stars.

Unfortunately, Gaia eDR3 proper motion (PM) measures exist for only ~ 200 stars in the system. They are mostly distributed along the brightest portion of blue disk population, and, because of their intrinsic faint magnitudes, the available astrometric measurements suffer from significant uncertainties (up to ~ 0.5 mas yr^{-1}). Therefore, to clean the observed CMD from field star interlopers, we performed a relative PM analysis. In Saracino et al. (2019) we have shown that it is possible to efficiently use GeMS images in combination with the HST data to derive reliable relative PMs also in dense GCs (see also Fritz et al. 2017). PMs obtained with these data sets have been

already used in Ferraro et al. (2021) and Pallanca et al. (2021). Here we detail the approach adopted to derive them.

We used the ACS/WFC and the GeMS+GSAOI data sets, which are separated by a temporal baseline of ~ 6.3 yr, as first and second epochs, respectively. PMs were derived by following the approach adopted by Saracino et al. (2019; see also Dalessandro et al. 2013). The procedure consists of determining the displacement of the centroids of the stars measured in the two epochs once a common coordinate reference frame is defined. The first step is to adopt a distortion-free reference frame, which we will call the master frame hereafter. The master-frame catalog contains stars measured in all the ACS/WFC I-band single exposures. Their coordinates were corrected for geometric distortions as described in Section 2. To derive accurate transformations between the second-epoch catalogs and the master catalog, we selected a sample of ~ 3300 bona fide stars having magnitude $20 < I_{DRC} < 24.5$ (corresponding approximately to magnitudes $13.0 < K_{DRC} < 18.5$), which we judged to be likely cluster members on the basis of their position in the CMD (i.e., stars distributed along the lower red giant branch (RGB), subgiant branch, and upper main sequence (MS)). We then applied a six-parameter linear transformation to report stars in the second-epoch catalogs to the master coordinate reference frame, by using the stars in common. We treated each chip separately, in order to maximize the accuracy. Moreover, we carefully corrected the coordinates of stars in the second-epoch catalogs for the important geometric distortions affecting the GSAOI camera by using the geometric distortion solutions published in Dalessandro et al. (2016).
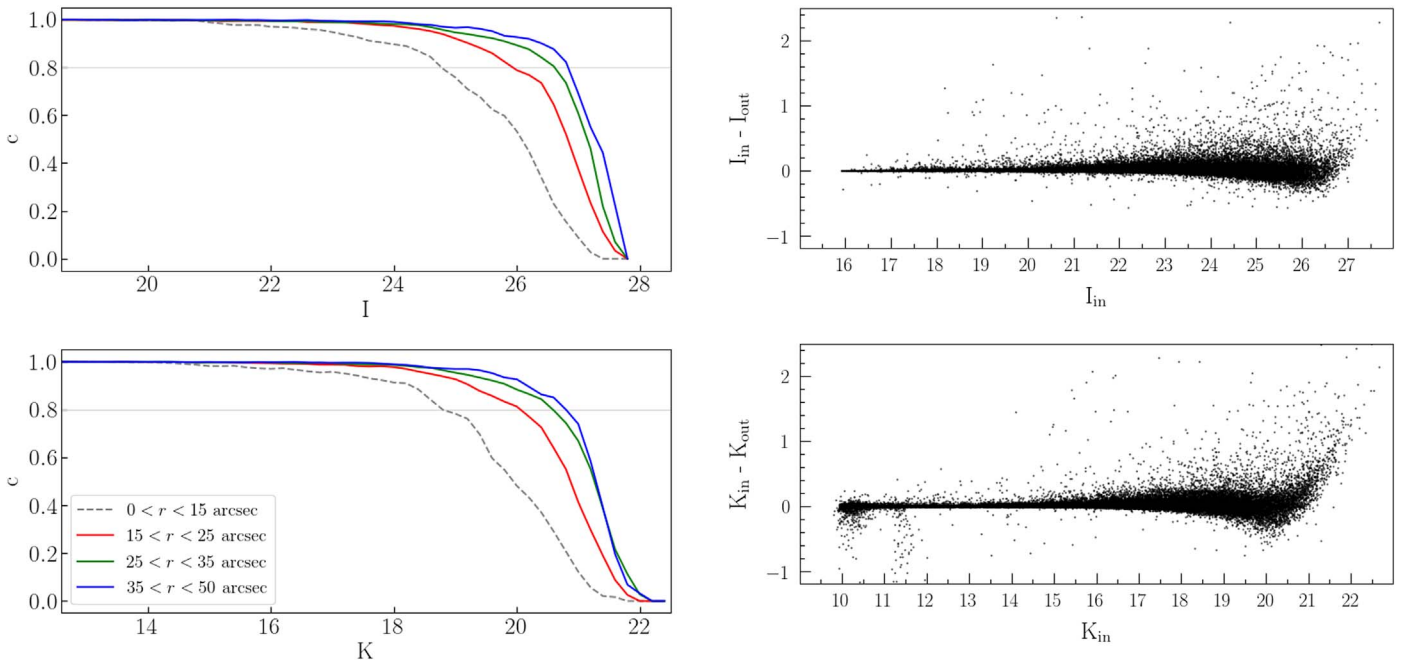
Figure 3. Left panels: completeness curves as a function of the I and K obtained in three concentric annuli at different cluster-centric distances. The horizontal gray lines mark the 80% completeness level for reference. Right panels: differences between the input and output magnitudes in the I and K bands (top and bottom panels, respectively) for the artificial stars recovered by the photometric analysis.

The mean position of a single star in each epoch (x_m, y_m) has been measured as the 3σ-clipped mean position calculated from all the N individual single-frame measurements. The relative rms of the position residuals around the mean value divided by $\sqrt{N}$ has been used as associated error (σ). Finally, the displacements are obtained as the difference of the positions (x_m, y_m) between the two epochs for all the stars in common. The error associated with the displacement is the combination of the errors on the positions of the two epochs. We should stress here that the first epoch is by construction in the same coordinate reference frame as the master catalog. The relative PMs (μ_x, μ_y) are finally determined by measuring the difference of the mean x and y positions of the same stars in the two epochs, divided by their temporal baseline $\Delta T = 6.3$ yr. Such displacements are in units of pixels yr^{-1}. We then iterated this procedure a few times by removing likely nonmember stars from the master reference frame based on the preliminary PMs obtained in the previous iterations. The convergence is assumed when the number of reference stars that undergoes this selection changes by less than $\sim$10% between two subsequent steps. At the end we derived relative PMs for 35,761 stars in the area where the HST and GeMS data sets overlap. The rightmost panels of Figure 2 show the derived vector point diagrams (VPDs) at different magnitude levels. As expected, the PM distributions get broader for increasing magnitudes because of the increasing uncertainties of the centroid positions of faint stars.

To build a clean sample of stars with a high membership probability, we defined for each magnitude bin a different fiducial VPD region centered on (0,0). The fiducial regions have radii of $3 \times \sigma$, where σ is the average PM error in that magnitude bin. The sample of stars thus selected corresponds to the observational catalog we will be using for the following analysis. The resulting CMD is shown in Figure 2(c), while panel (b) shows the CMD of likely field stars that have been excluded.

Because of the partial overlap between the motion of Liller 1 and that of bulge and disk stellar populations in this region of

the galaxy, a possible residual contamination also is expected in the PM-cleaned CMDs. As a sanity check, we estimated the fraction of not accounted for field populations by using the "Besançon model of stellar population synthesis of the galaxy" (Robin et al. 2003). We retrieved the output of the model in the direction of Liller 1 for a solid angle corresponding to the area sampled by the Gemini data ($95'' \times 95''$; Section 2). Following the PM selection described before, we selected stars moving with the same transverse velocity components as Liller 1 $(\mu_\alpha \cos\delta, \mu_\delta) = (-5.403, -7.431)$ mas yr^{-1}; from Vasiliev & Baumgardt 2021) within a tolerance range corresponding to the $3 \times \sigma$ selection adopted in Figure 2. In the Besançon simulation we find 2635 residual contaminating stars out of 22,861 Liller 1 observed member stars (i.e., selected as members based on our analysis). If we then limit this comparison to the turn-off region $(24 < I_{\rm DRC} < 25)$, we find $\sim$490 residual contaminating stars in the Besançon model out of 7447 likely member stars, thus yielding a residual contamination of $\sim$6%. We therefore expect a negligible impact of such a small residual contamination on the following analysis.

4. Artificial Star Experiments

For the reconstruction of the SFH of Liller 1, an accurate determination of photometric errors and incompleteness of the adopted data is needed. To this aim, we performed extensive artificial star experiments following the approach described in Dalessandro et al. (2015) with some ad hoc modifications that are detailed below. We generated a catalog of simulated stars with an I-band input magnitude $(I_{\rm in})$ extracted from a flat luminosity function (LF) extrapolated beyond the observed limiting magnitude in the $(I-K, I)$ observed CMD. Then, to each star extracted from the LF, we assigned an input K magnitude $(K_{\rm in})$ from a randomly extracted value of color in the interval $2 < (I-K) < 9$ to homogeneously sample the range of magnitudes and colors occupied by stars in the observed CMD. We note that this is a
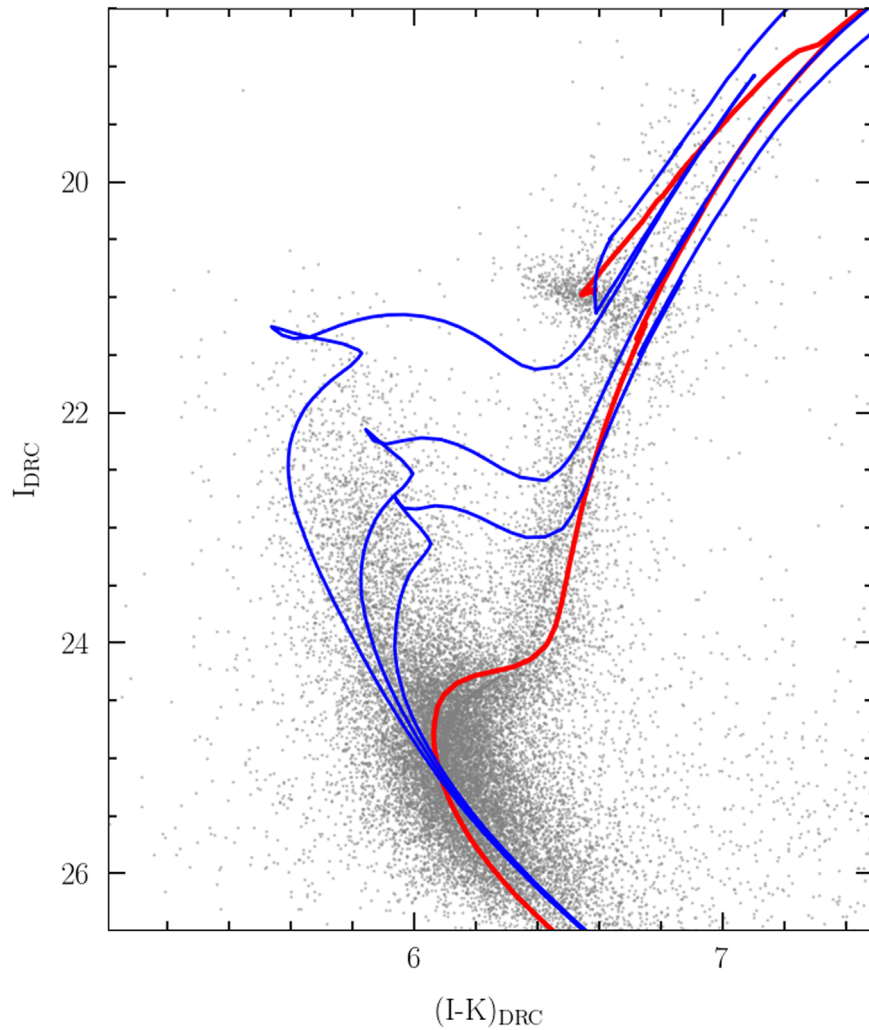
Figure 4. Sample of isochrones overplotted to the differential reddening-corrected and PM-selected CMD of Liller 1 (gray dots): in red the 12 Gyr old isochrone with [M/H] = −0.3 that nicely reproduces the old stellar population; in blue three young isochrones (of 1, 2, and 3 Gyr, from top to bottom) at larger metallicity [M/H] = +0.3, which are needed to reproduce the locus occupied by the young population.

critical aspect for the present analysis and it differs from the approach adopted in previous papers of our group and from what was done in Ferraro et al. (2021), where artificial stars follow the mean loci of the main evolutionary sequences defined by the observations.

We then added artificial stars to real images adopting the same PSF models resulting from the photometric analysis by means of the `DAOPHOTIV/ADDSTAR` package. Artificial stars were placed into the images in such a way they follow the stellar density profile obtained by Saracino et al. (2015) for Liller 1. To avoid artificial crowding, stars were placed in a regular grid composed by 20×20 pixel cells (which correspond to ∼10 times the stellar FWHM in the HST images), where only one artificial star was allowed to lie. In this way, for each run we could add a maximum number of ∼5000 artificial stars. We repeated this analysis several times to reach a final simulated catalog composed of more than 350,000 artificial stars, which is about 6 times larger than the number of observed stars. For each iteration, we performed the same photometric analysis described in Section 2. Those stars recovered after the photometric analysis have also values for I_{out} and K_{out}.

The completeness is then defined as the ratio between the number of recovered artificial stars and that of the injected ones. Specifically, a star was not counted if it was not recovered during the photometric reduction, it was not included in the common ACS/WFC and GeMS field of views or it had a 0.75 brighter magnitude than its input to exclude cases where an artificial star is placed in the same spatial position as a real one with the same or brighter magnitude. The left panels of Figure 3 show the completeness curves as a function of both the I and K bands and obtained for four concentric annuli at different cluster-centric distances. The right panels show the distributions of $(I_{in}–I_{out})$ and $(K_{in}–K_{out})$ as a function of the input I and K bands, respectively. These distributions are used to quantify the photometric errors and the fraction of possible blends as a function of the magnitude and color.

5. The Star Formation History Analysis

5.1. The Method

Figure 4 shows a zoomed view of the DRC and PM-selected CMD of Liller 1. To guide the eye we superimposed a set of isochrones of different ages retrieved from the PARSEC database (Bressan et al. 2012). We adopted a distance modulus
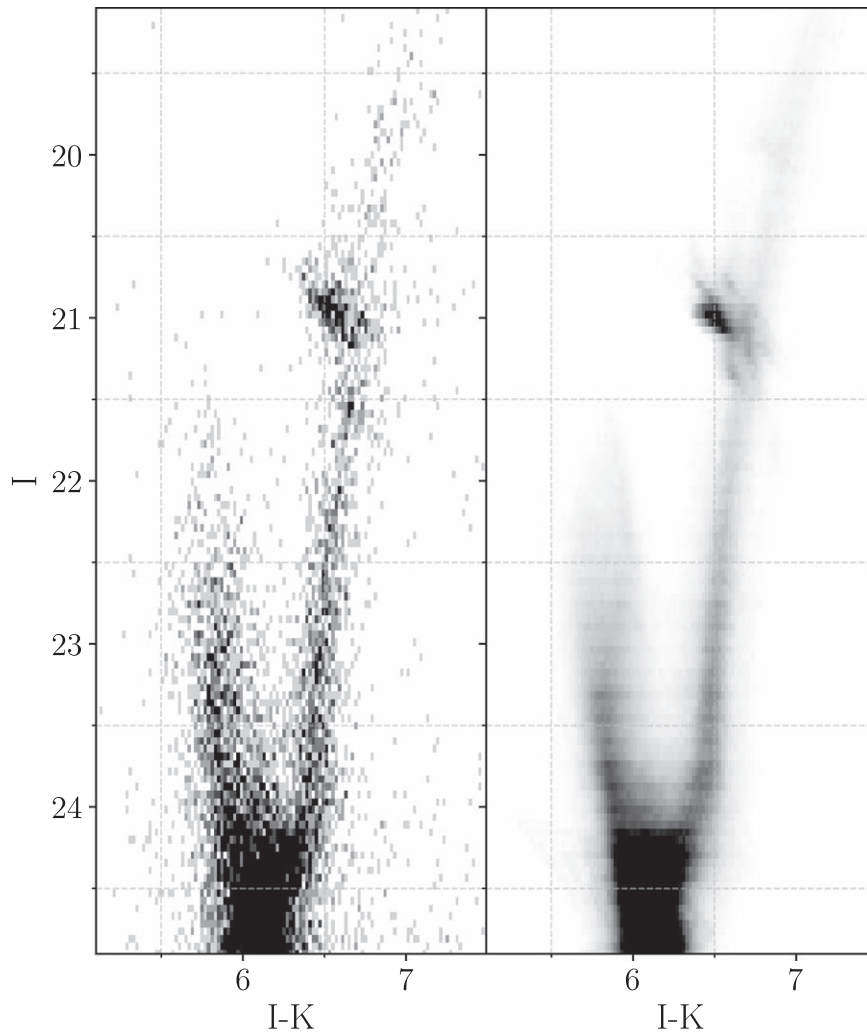
Figure 5. Hess diagrams for the observed CMD (left) and the best-fit synthetic CMD (right).

$(m$–$M)_0 = 14.65$ and extinction $E(B$-$V) = 4.52$ (Ferraro et al. 2021) to match the models to the observations. For the extinction law we adopt Cardelli (1989) with a total-to-selective extinction value $R_V = 2.5$, as suggested by Pallanca et al. (2021). As already found by Ferraro et al. (2021), such a simple comparison shows that the bulk population of Liller 1 is grossly reproduced by a model with subsolar metallicity ([Fe/H] $\sim - 0.3$) with an age $t = 12.0 \pm 1.5$ Gyr and by a more metal-rich ([Fe/H] $\sim + 0.2$) and significantly younger population with age ranging from $\sim$3 to $\sim$1 Gyr. These results broadly indicate that Liller 1 might have experienced at least two episodes of star formation, with the second one possibly having formed stars from a more metal-rich gas.

Here we attempt to move a step forward and to characterize in detail the stellar populations observed in Liller 1 and their SFH.

The SFH was determined using the population synthesis routine Star Formation Evolution Recovery Algorithm (SFERA; Cignoni et al. 2015), applied to the differential reddening and PM-cleaned CMD shown in Figure 4. SFERA employs a synthetic CMD method, along the lines pioneered by Tosi et al. (1991). We provide here only a short description of SFERA's approach, and we refer the reader to Cignoni et al. (2015, 2016, 2018) for further details. Briefly, SFERA builds a library of synthetic CMDs starting from a set of theoretical models spanning a wide range of parameters including age, metallicity, stellar initial mass function

(IMF), binary fraction, and a range of distance and extinction values. The model CMDs are then convolved with observational errors and biases as measured from artificial star tests. Finally, SFERA employs maximum likelihood statistics to compare synthetic and observed CMDs and recover the most likely SFH.

Synthetic CMDs are generated by using isochrones from the PARSEC–COLIBRI (Bressan et al. 2012; Marigo et al. 2017) stellar evolution models. In particular, all synthetic CMDs are Monte Carlo realizations of all possible combinations of 14 equally spaced age bins, between the youngest (2 Myr) and the oldest available isochrone (13.4 Gyr). Within each age bin, a range of metallicities is allowed, from the lowest available metallicity, [M/H] $= - 2.0$, to the highest, [M/H] $= + 0.3$.[10] This metallicity range has been chosen to include the available metallicity derivations of Liller 1 and, at the same time, to secure a quite large tolerance for the iron abundance to vary. IR high-resolution spectroscopy has been obtained with NIR-SPEC@Keck (Origlia & Rich 2002) for only a handful of stars. This analysis suggests an average value of about half solar metallicity and some α-enhancement ([α/Fe] $\sim + 0.3$). A Kroupa (2001) IMF between 0.1 and 300 $M_\odot$ is then used to fully populate the synthetic CMDs. The adoption of other

---

[10] We adopt [M/H]=$\log(Z/Z_\odot)$, with $Z_\odot = 0.0152$. We report also that [M/H]=[Fe/H] + $\lg(0.638*10^{[\alpha/Fe]} + 0.362)$ as in Salaris et al. (1993).
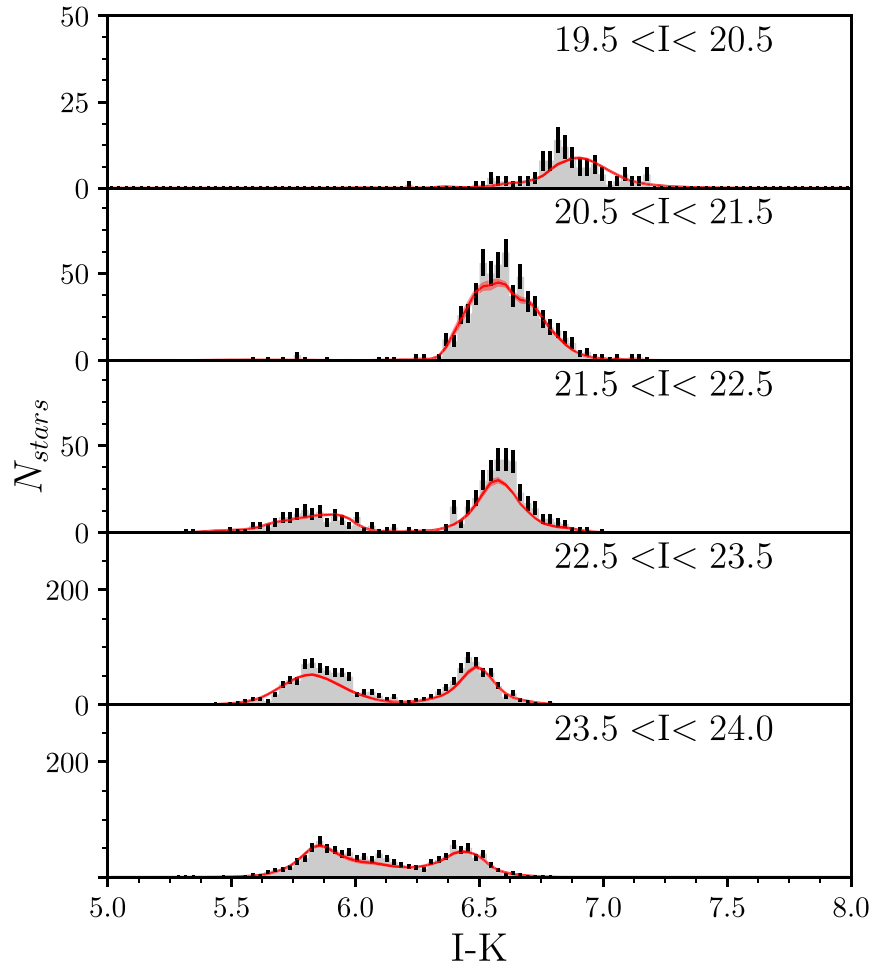
Figure 6. Observed color distributions of Liller 1 in four magnitude bins (gray shaded areas), compared to those obtained from our best-fit SFH solution (red lines). The black vertical segments correspond to the Poissonian error in each color bin, while the uncertainty in the synthetic distribution is marked by the red shaded areas.

commonly used IMFs, such as Salpeter (1955) or Chabrier (2003) IMFs, is expected not to impact significantly the main results of the present analysis. In fact, the quoted IMFs do not differ significantly for stellar masses larger than $\sim 1 M_\odot$, which is approximately the mass regime we focus on. Unresolved binaries are also considered and 30% of synthetic stars are coupled with a stellar companion sampled from the same IMF.

Distance and foreground extinction are also free parameters, whereas differential extinction is not considered as it has been corrected star by star as discussed above in the observations.

To properly compare synthetic CMDs with the observed ones, we need to convolve theoretical models with all the observed sources of uncertainties, such as photometric errors, blends, and photometric incompleteness. We account for observational errors and incompleteness by smearing the synthetic CMDs with the color and magnitude distribution of errors and completeness derived from our artificial star tests (Section 4).

To derive the SFH and identify the best-fit model, SFERA first constructs a Hess diagram for the observed data, and then attempts to match this by linearly combining Hess diagrams from our library of synthetic CMDs. The best combination of model Hess diagrams is then obtained minimizing a Poissonian likelihood (function of the data-model residuals) by means of a hybrid-genetic algorithm.

The severe crowding conditions of the innermost regions of Liller 1 hindered the possibility to effectively use the turn-off

region for the entire available FOV. For this reason we decided to limit the SFH analysis to stars at cluster-centric distances larger than 15″, where the photometric completeness is generally larger than 80% for $I \sim 25$ (see Figure 3). We estimate that with such a selection we sample $\sim$40% of the total mass of Liller 1.

5.2. The Best-fit SFH

SFERA estimated a best-fit extinction corrected distance modulus of 14.65 and foreground reddening of $E(B - V) = 4.52$. These values nicely compare with those previously derived by Ferraro et al. (2021) and Pallanca et al. (2021).

In Figure 5 we compare the observed and the best-fit synthetic CMDs (left and right panels, respectively) by showing their Hess diagrams for a first visual check. At a qualitative analysis, the synthetic CMD indeed nicely reproduces the main features of the observed one. In fact, it matches the observed turn-off, the color and magnitude extension of the blue plume, and the RGB color width, as well as the color extension and inclination of the red clump (RC).

For a more quantitative analysis, in Figure 6 we directly compare the color distributions obtained from the observed and the best-fit synthetic CMDs in four magnitude bins. The best-fit synthetic CMD reproduces fairly well the mean color and the
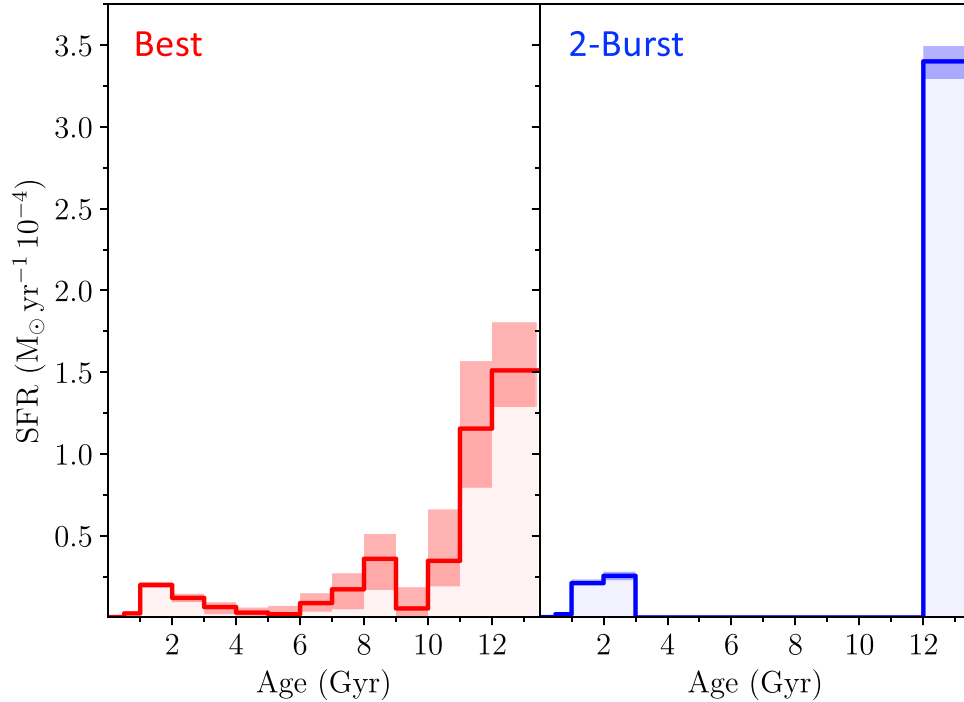
Figure 7. Best (red) and 2-burst (blue) SFHs of Liller 1. The shaded areas define the regions between the 5th and 95th percentile values.

width of all the main observed evolutionary sequences, even if in the mid-/bright portion of the RGB and along the young MS ($21.5 < I < 23.5$) the best-fit synthetic CMD tends to slightly underpredict the number of observed stars. This difference can be ascribed to residual contamination from bulge + disk stars along the line of sight (see Section 3) and to a slight overestimate of the photometric completeness at the turn-off magnitude level of the old population ($I \sim 25$), which then produces smaller number counts at brighter magnitudes in the synthetic CMDs.

The resulting best-fit SFH is shown in red in Figure 7. The boundaries of the light-red shaded rectangles correspond to the 5th and 95th percentile values of the distribution of all the synthetic CMDs produced by SFERA and compared with the observations. The first key result emerging from Figure 7 is that Liller 1 has been active in forming stars over the entire Hubble time. More specifically, three SF episodes are clearly detected: (1) a dominant one, occurring 12–13 Gyr ago with a tail extending for up to ~3 Gyr; (2) an intermediate burst, between 6 and 9 Gyr ago; (3) a recent one, between 1 and 3 Gyr ago. In addition, our analysis shows robustly that about 1 Gyr ago Liller 1 stopped forming stars. It is worth stressing here that we can exclude that this result arises because of saturation issues. In fact, saturation appears to become important at $I_{DRC} < 19$, which is more than 3 magnitudes brighter than the turn-off magnitude of the 1 Gyr population.

In the best-fit recovered SFH, we find a broadly bimodal metallicity distribution (see Figure 8). The stellar metallicity mostly fluctuates in the range $-0.8 < [M/H] < -0.4$ dex at the older epochs, then it increases with time, and the metallicity of the younger populations ($t < 3$ Gyr) peaks at $[M/H] \sim +0.2$ (Figure 9).

The cumulative mass distribution related to such an SFH is presented in Figure 10. It shows that more than ~70% of the total mass was produced during the first event of SF ($t > 10$ Gyr), thus confirming that the bulk population of Liller 1 is old

(Ferraro et al. 2021). The remaining ~30% is then almost equally split between the second and third SF events, with the latter producing no more than ~10% of the total mass. We should recall at this point that the fraction of mass produced in the last 3–4 Gyr might be underestimated because of the radial selection adopted to perform the analysis. In fact, the younger stellar population of Liller 1 is more centrally concentrated than the older ones and the number ratios between the young and old populations is 0.98 ± 0.04 and 0.66 ± 0.02 for distances smaller and larger than $15''$, respectively (see Ferraro et al. 2021). We also stress here that, while blue straggler stars overlap with the distribution of young stars in the CMD, they have only a limited impact on the recovered SFH of the young component (<3 Gyr) as they are expected to represent 5%–10% of the total number of the blue plume population (see Ferraro et al. 2021 for details about the number counts).

5.3. Alternative SFH Solutions

We tested the possible impact of poorly modeled observational uncertainties on the recovered SFH and in particular on the results related to the older component where they can be more important because of the poorer ability to effectively distinguish populations with relatively small age differences. More specifically, we checked whether the old and the intermediate SF episodes can be safely considered as two separate events and whether the resulting nonnegligible duration (~3 Gyr) of the old SF episode is real. To this aim, we reperformed the SFH analysis by imposing a 2-burst solution in which the first SF episode is older than 12 Gyr and the more recent one is younger than 3 Gyr. The resulting SFH (blue slope) is compared with the previous one (red slope) in Figure 7. The Hess diagram and the color number count distribution corresponding to the newly derived SFH are shown in Figure 11 and Figure 12, respectively. Although a reasonable match between the observed and the synthetic CMDs seems to
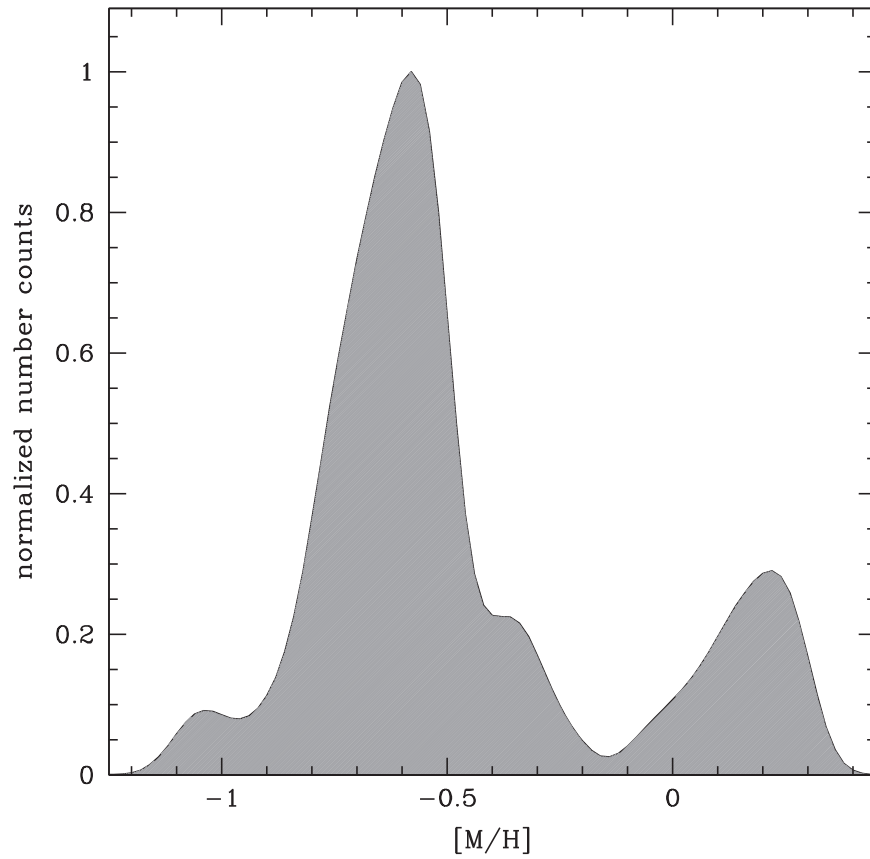
Figure 8. Generalized histogram of the metallicity distribution of Liller 1 as constrained from the best-fit SFH.
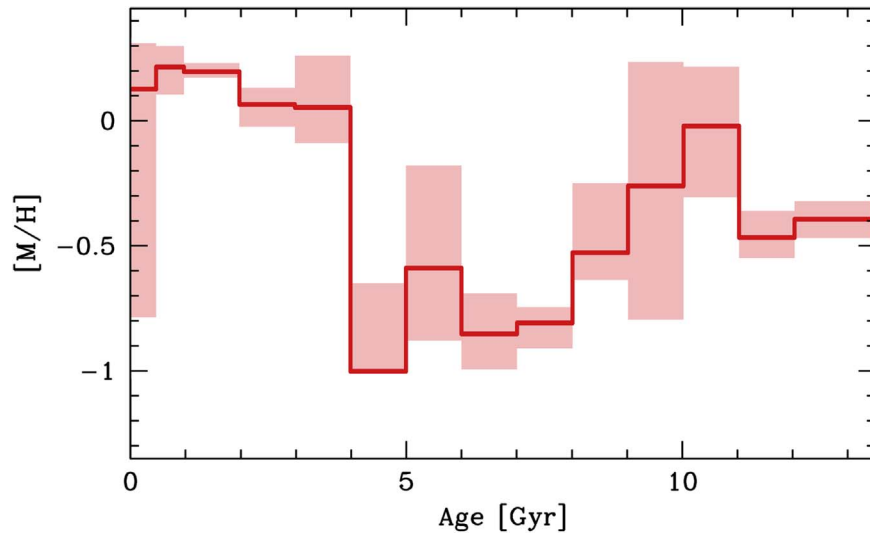

Figure 9. Age–metallicity distribution as recovered from the best-fit SFH. The shaded areas corresponds to the 5th and 95th percentile values.

be achieved also in this case, a closer look shows that the two SFHs show nonnegligible differences in specific CMD regions.

First, we note that when only two episodes of SF are assumed, the RC gets more horizontal than the observations and does not provide an adequate match to the observed color and magnitude distributions. In Figure 13 we compare the CMD star density distributions in the RC region of the difference between the observations and the two SFH solutions. Clearly, in the case of an SF with two discrete bursts the residuals gets larger and more structured. The main responsible

for such a mismatch is likely the lack of stars with ages in the range 7–12 Gyr and likely more metal-rich than the old component.

In addition, we note that the 2-burst SFH solution provides a worse match of the young population MS distribution ($I < 24$, $I–K < 6.3$). In Figure 14, we compare the differential and cumulative LFs obtained from the observations (black line), with that resulting from the two SFH solutions (red and blue). The LF obtained with the best-fit SFH provides a better match of the observations. A K-S test on the cumulative LF
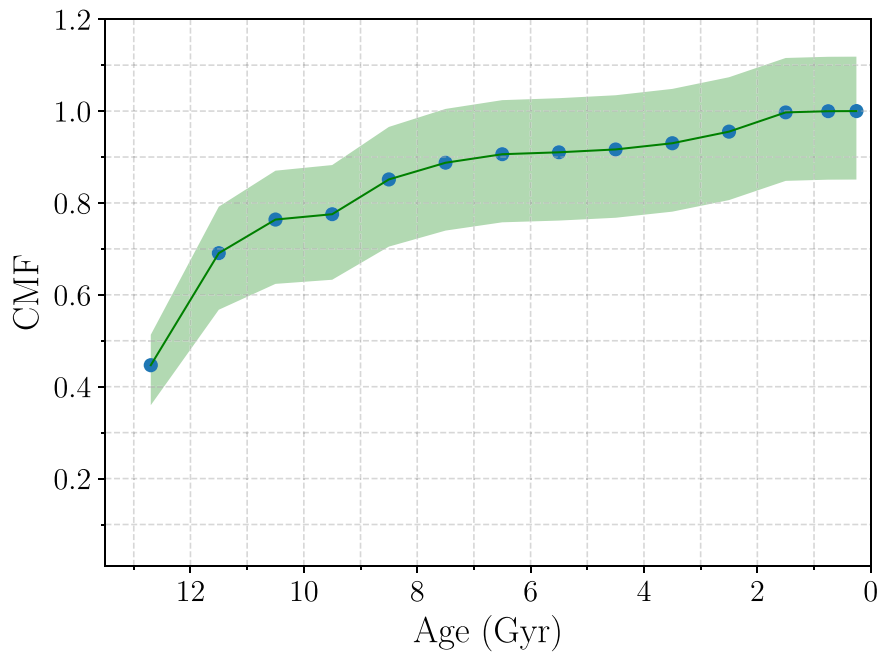
Figure 10. Cumulative mass distribution for the recovered SFH.
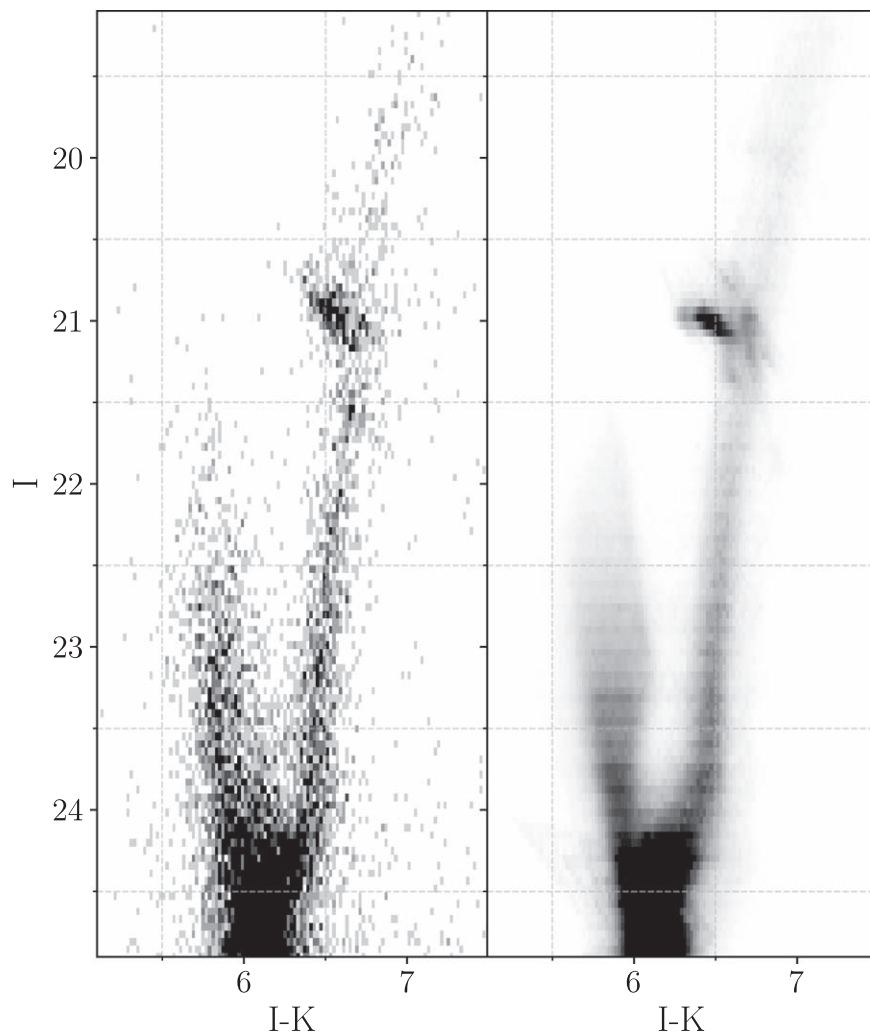
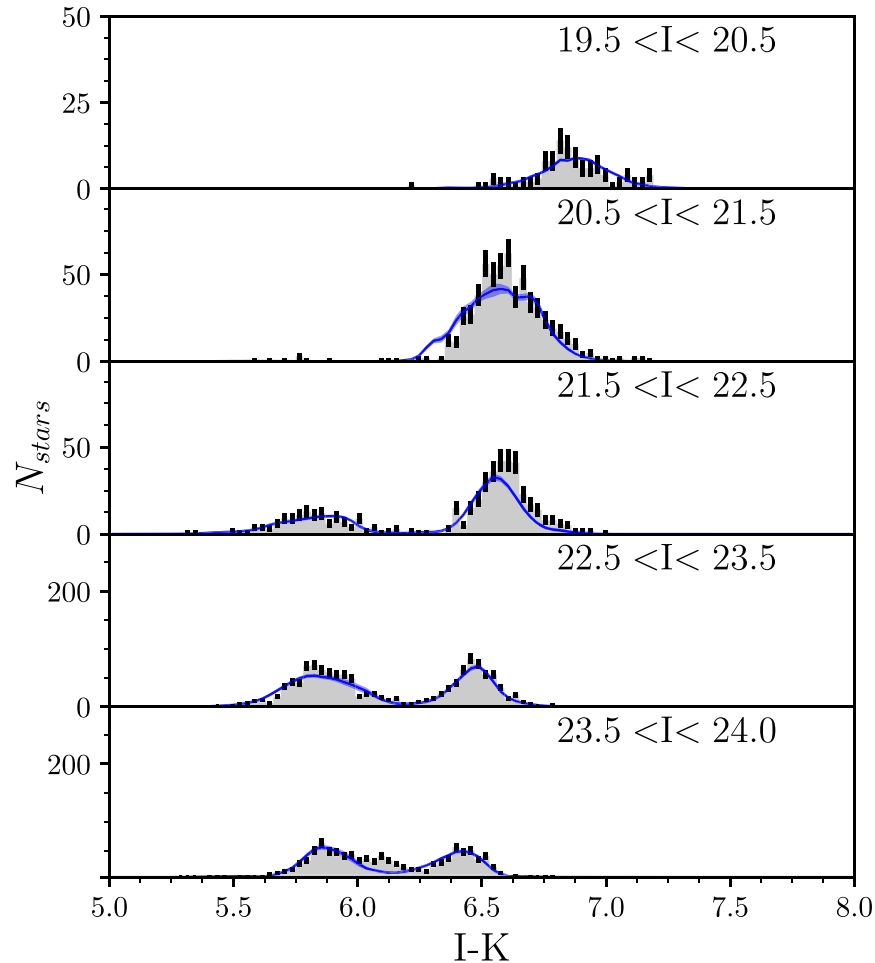**Figure 11.** As in Figure 5, but now for the 2-burst SFH solution.

Figure 12. As in Figure 6, but now for the 2-burst SFH solution.

demonstrates that the 2-burst LF is extracted from a different parent distribution than the observed one with a high degree of confidence ($P_{KS} \sim 5 \times 10^{-3}$).

Therefore, although we cannot completely exclude that the SFH of Liller 1 is bimodal and characterized by a very narrow old SF episode, we stress that an SFH history with three episodes, and characterized by a first event with possibly an extended tail, followed by an intermediate and a young SF episode, provides an overall better match to the observations.

6. Summary and Conclusions

Liller 1 and Terzan 5 are without a doubt among the most peculiar and interesting stellar systems in the Milky Way, and their origin is still strongly debated. Their present-day properties, such as their chemical abundance patterns and their similarity with those of the Galactic bulge (Ferraro et al. 2009; Origlia & Rich 2011), their present-day orbits (Massari et al. 2015), as well as their age–metallicity relations (Pfeffer et al. 2021) would suggest they are genuine Galactic stellar systems and would exclude that they are the remnants of an external massive stellar system accreted by the Milky Way, like a dwarf galaxy (e.g., Tolstoy et al. 2009) or its nuclear star cluster (e.g., Neumayer et al. 2020).

Two main ideas have been put forward for their formation. One suggests that Terzan 5 and Liller 1 are the remnants of primordial massive systems, likely produced by the fragmentation of an early disk, that formed in situ and contributed to generate the bulge some 12 Gyr ago, the so-called bulge fossil fragments (Ferraro et al. 2009; Ferraro et al. 2021). The detection of similar structures in the star-forming regions of high-redshift galaxies confirms that such massive fragments likely existed at the epoch of the Milky Way assembly. The second scenario suggests that both Liller 1 and Terzan 5 are the result of a relatively recent encounter between an old and massive GC formed in the bulge and a GMC orbiting the Galactic disk (Bastian & Pfeffer 2022). Such an encounter should have been able to provide the necessary gas reservoir for the formation of the young populations observed in these systems (McKenzie & Bekki 2018).

The latter scenario is expected to produce two discrete and well-separated SF episodes. Hence, to shed new light on the physical mechanisms driving the formation of Liller 1 and Terzan 5, in this paper we present the first detailed analysis of the SFH of Liller 1. To this aim, we have used deep optical HST and IR GeMS/GSAOI data used in combination with a synthetic CMD analysis to derive the SFH of the system. The best-fit solution suggests that Liller 1 has been actively forming stars almost for its entire lifetime and we can identify three SF episodes. The main episode started 12–13 Gyr ago with a tail extending for up to ~3 Gyr. This SF event is responsible for ~70% of the present-day total mass of Liller 1. The second peak occurred between 6 and 9 Gyr ago contributing to an additional ~15% of the system's mass. The most recent event
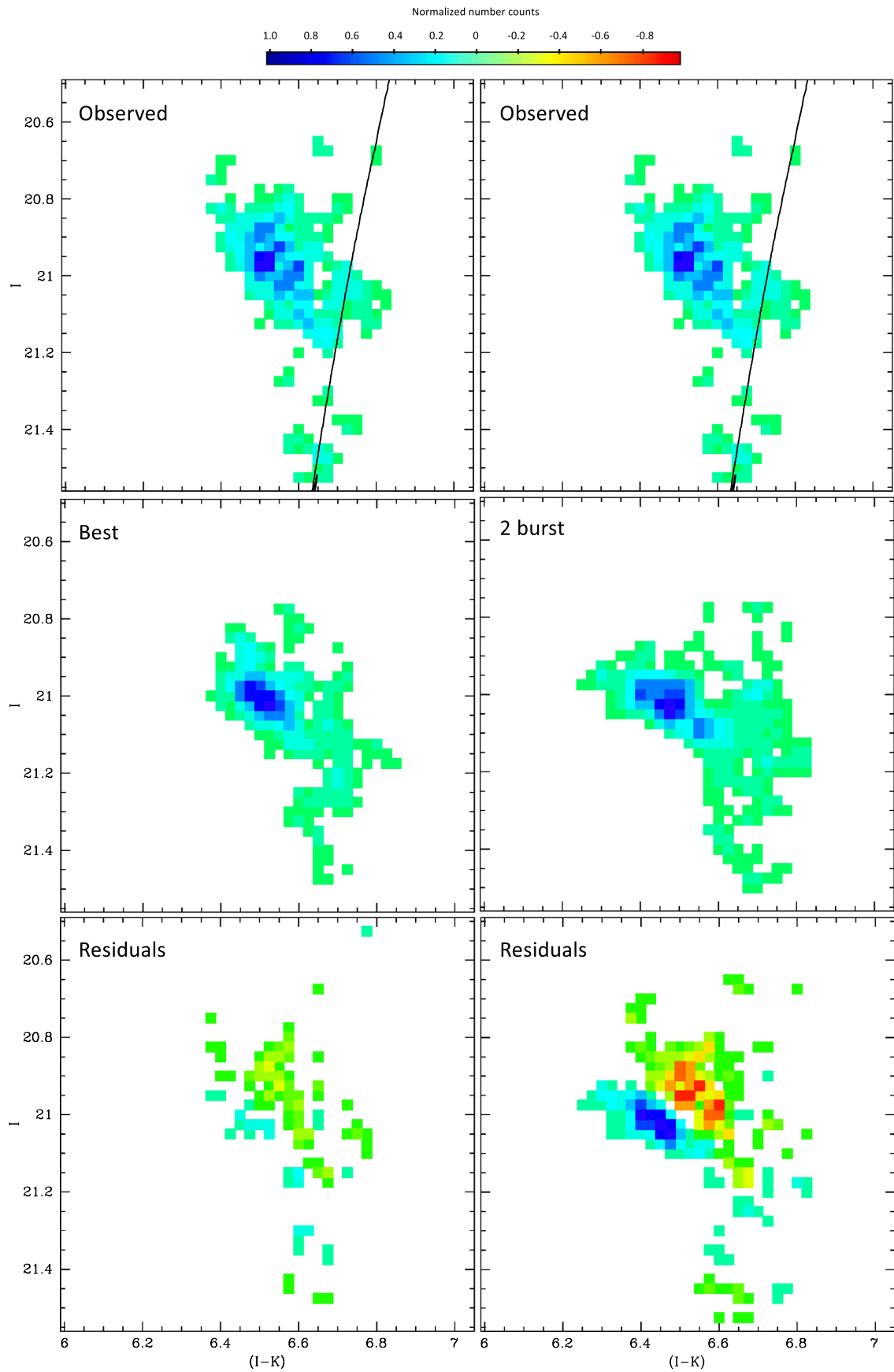
Figure 13. Upper panels: 2D distribution of the observed CMD density number counts in the red clump region. Middle panels: distributions of the synthetic stars as obtained from the best-fit and 2-burst SFH solutions. Lower panels: CMD distribution of the difference between the number of observed and synthetic stars.
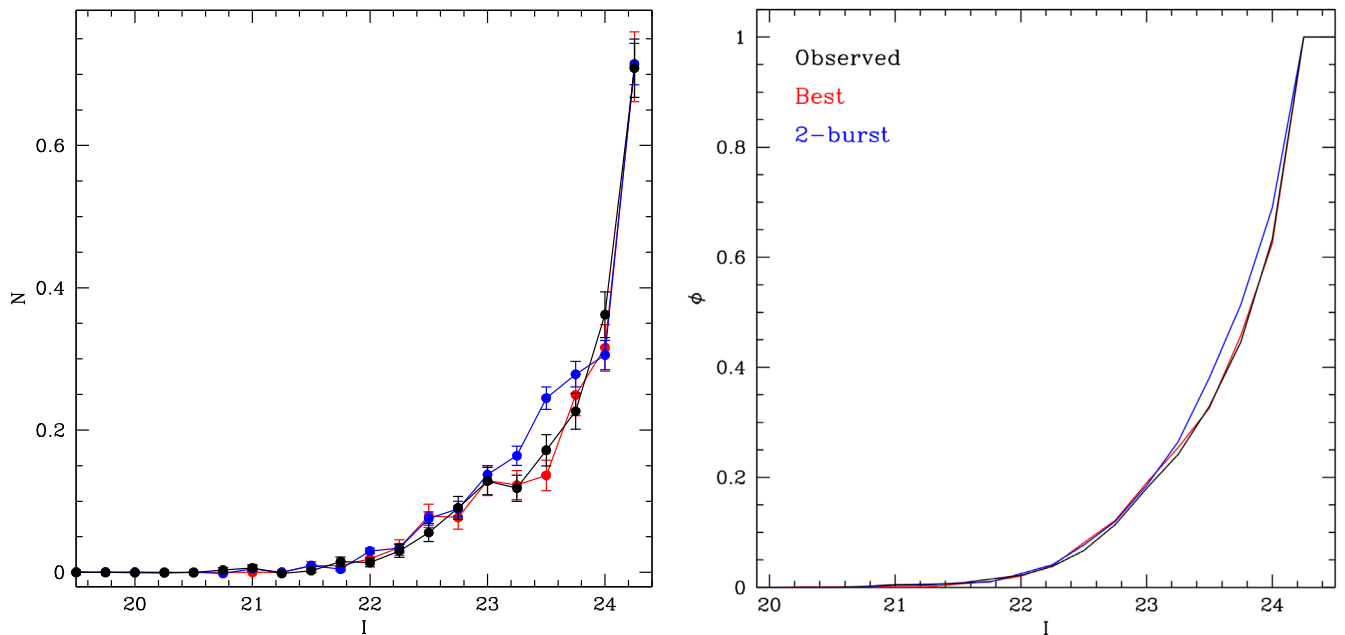
Figure 14. Left panel: normalized luminosity functions of the young MS population (I < 24, *I*–*K* < 6.3). In black is the observed distribution, while the red and blue curves refer to the best and 2-burst SFH solutions. Right panel: as before, but for the cumulative luminosity functions.

started some 3 Gyr ago and stopped ∼1 Gyr ago, when a quiescent phase started. Our analysis shows that the young population contributes at least to ∼10% of the total mass of Liller 1. We also find that the best match with the observations is obtained by assuming a global average metallicity [M/H] = −0.5 for the older stars, in quite good agreement with the few spectroscopic abundance measurements available in the literature (Origlia & Rich 2002), and with [M/H] ∼ +0.2 for stars that were born in the last ∼3 Gyr.

If we take the results of our analysis at a face value, we should conclude that the overall SFH complexity, the long time over which Liller 1 has been forming stars, and the number of SF episodes suggest that Liller 1 unlikely formed through the merger between an old globular cluster and a GMC, as recently proposed by Bastian & Pfeffer (2022). On the contrary, our findings provide further support to the idea that Liller 1 is the surviving relic of a much more massive primordial structure, the so-called bulge fossil fragments, that contributed to the Galactic bulge formation. In this respect, it is worth stressing that stellar systems with original stellar masses larger than several $10^6 M_\odot$ are expected (see Bailin & Harris 2009) to be able to retain a fraction of their SN ejecta even without the additional contribution of a dark matter halo, thus providing further support to the self-enrichment scenario. Counter examples based on unresolved stellar populations as suggested by Bastian & Pfeffer (2022) can be biased by the uncertainties arising from the derivation of masses and stellar population properties from integrated quantities. Moreover, it is also questionable that the sole analysis of the integrated properties of Terzan 5 and Liller 1 could reveal their complexity and true nature. Bastian & Pfeffer (2022) discuss the caveat that massive systems (such as Liller 1 and Terzan 5) in the dense inner galaxy may be able to capture field stars characterized by a range of metallicities and ages. However, the expected number of captured stars is still small (of the order of a few percent), while the extended SF of Liller 1 contributes to more than 30%

of its present-day mass. We should also note that the age spread needed to best-fit the old stellar population is not compatible with the assumption that it was originally a genuine GC. On the same line, the extended duration of the young SF event (Δt ∼ 2–3 Gyr) appears to be hardly compatible with the encounter between a GMC and a massive GC.

We performed an ad hoc simulation including "by hand" only two SF episodes at t ∼ 12 Gyr and t < 3 Gyr. Although the CMD derived by using this approach is still broadly compatible with the data, we find that the specific number count distribution of the RC and young MS in the CMD (Figure 13 and 14) cannot be properly reproduced with such a configuration, but they are better fit by adopting a larger number of SF events lasting for a longer time.

Our group is now conducting an extensive observational effort to obtain high-resolution spectroscopy of Liller 1 to probe the chemical abundance patterns of this system on a statistically significant sample possibly including the young population. This will certainly provide critical information to move the SFH analysis of this system to another step of detail. On the same line, we are planning to apply the same analysis to the case of Terzan 5 and then compare the results between the two systems.

ORCID iDs

Emanuele Dalessandro ⓘ https://orcid.org/0000-0003-4237-4601
Michele Cignoni ⓘ https://orcid.org/0000-0001-6291-6813
Francesco R. Ferraro ⓘ https://orcid.org/0000-0002-2165-8528
Barbara Lanzoni ⓘ https://orcid.org/0000-0001-5613-4938
Livia Origlia ⓘ https://orcid.org/0000-0002-6040-5849
Cristina Pallanca ⓘ https://orcid.org/0000-0002-7104-2107
Sara Saracino ⓘ https://orcid.org/0000-0003-4746-6003
Elena Valenti ⓘ https://orcid.org/0000-0002-6092-7145

References

Anderson, J., & Bedin, L. R. 2010, PASP, 122, 1035
Bailin, J., & Harris, W. E. 2009, ApJ, 695, 1082
Bastian, N., & Pfeffer, J. 2022, MNRAS, 509, 614
Behrendt, M., Burkert, A., & Schartmann, M. 2016, ApJL, 819, L2
Bellini, A., Piotto, G., Bedin, L. R., et al. 2009, A&A, 493, 959
Bournaud, F. 2016, in Galactic Bulges, ed. E. Laurikainen, R. Peletier, & D. Gadotti (Cham: Springer), 355
Bressan, A., Marigo, P., Girardi, L., et al. 2012, MNRAS, 427, 127
Cardelli, J. A., Clayton, G. C., & Mathis, J. S. 1989, ApJ, 345, 245
Carollo, C. M., Scarlata, C., Stiavelli, M., et al. 2007, ApJ, 658, 960
Chabrier, G. 2003, PASP, 115, 763
Cignoni, M., Sabbi, E., & van der Marel, R. P. 2015, ApJ, 811, 76
Cignoni, M., Sabbi, E., & van der Marel, R. P. 2016, ApJ, 833, 154
Cignoni, M., Sacchi, E., Aloisi, A., et al. 2018, ApJ, 856, 62
Cowie, L. L., Hu, E. M., & Songaila, A. 1995, AJ, 110, 1576
Dalessandro, E., Ferraro, F. R., Massari, D., et al. 2013, ApJ, 778, 135
Dalessandro, E., Ferraro, F. R., Massari, D., et al. 2015, ApJ, 810, 40
Dalessandro, E., Saracino, S., Origlia, L., et al. 2016, ApJ, 833, 111
Dalessandro, E., Zocchi, A., Varri, A. L., et al. 2018, MNRAS, 474, 2277
Dekel, A., Sari, R., & Ceverino, D. 2009, ApJ, 703, 785
Elmegreen, B. G., Bournaud, F., & Elmegreen, D. M. 2008, ApJ, 688, 67
Elmegreen, D. M., Elmegreen, B. G., & Elmegreen, T. E. 2005, ApJL, 623, L71
Elmegreen, D. M., Elmegreen, B. G., & Hirst, A. C. 2004, ApJL, 604, L21
Ferraro, F. R., Dalessandro, E., Mucciarelli, A., et al. 2009, Natur, 462, 483
Ferraro, F. R., Pallanca, C., Lanzoni, B., et al. 2021, NatAs, 5, 311
Ferraro, F. R., Sollima, A., Pancino, E., et al. 2004, ApJL, 603, L81
Fritz, T. K., Linden, S. T., Zivick, P., et al. 2017, ApJ, 840, 30
Gaia Collaboration, Brown, A. G. A., Vallenari, A., et al. 2021, A&A, 649, A1
Genzel, R., Newman, S., Jones, T., et al. 2011, ApJ, 733, 101
Giavalisco, M., Steidel, C. C., & Macchetto, F. D. 1996, ApJ, 470, 189
Gonzalez, O. A., Zoccali, M., Vasquez, S., et al. 2015, A&A, 584, A46
Immeli, A., Samland, M., Gerhard, O., et al. 2004, A&A, 413, 547
Johnson, C. I., & Pilachowski, C. A. 2010, ApJ, 722, 1373
Johnson, C. I., Rich, R. M., Kobayashi, C., et al. 2013, ApJ, 765, 157
Kroupa, P. 2001, MNRAS, 322, 231
Lee, Y.-W., Joo, J.-M., Sohn, Y.-J., et al. 1999, Natur, 402, 55
Majewski, S. R., Patterson, R. J., Dinescu, D. I., et al. 2000, in The Galactic Halo: From Globular Cluster to Field Stars, Proc. of the 35th Liege International Astrophysics Coll., ed. A. Noels et al. (Liege: Univ. Liege), 619
Marigo, P., Girardi, L., Bressan, A., et al. 2017, ApJ, 835, 77
Massari, D., Dalessandro, E., Ferraro, F. R., et al. 2015, ApJ, 810, 69
Massari, D., Koppelman, H. H., & Helmi, A. 2019, A&A, 630, L4
Massari, D., Mucciarelli, A., Ferraro, F. R., et al. 2014, ApJ, 795, 22
McKenzie, M., & Bekki, K. 2018, MNRAS, 479, 3126
Minniti, D., Lucas, P. W., Emerson, J. P., et al. 2010, NewA, 15, 433
Neichel, B., Rigaut, F., Vidal, F., et al. 2014, MNRAS, 440, 1002
Ness, M., Freeman, K., Athanassoula, E., et al. 2013, MNRAS, 430, 836
Neumayer, N., Seth, A., & Böker, T. 2020, A&ARv, 28, 4
Norris, J. E., Freeman, K. C., & Mighell, K. J. 1996, ApJ, 462, 241
Origlia, L., Rich, R. M., & Castro, S. 2002, AJ, 123, 1559
Origlia, L., Rich, R. M., Ferraro, F. R., et al. 2011, ApJL, 726, L20
Pallanca, C., Ferraro, F. R., Lanzoni, B., et al. 2021, ApJ, 917, 92
Pancino, E., Ferraro, F. R., Bellazzini, M., et al. 2000, ApJL, 534, L83
Pfeffer, J., Lardo, C., Bastian, N., Saracino, S., & Kamann, S. 2021, MNRAS, 500, 2514
Queiroz, A. B. A., Anders, F., Chiappini, C., et al. 2020, A&A, 638, A76
Robin, A. C., Reylé, C., Derrière, S., et al. 2003, A&A, 409, 523
Rojas-Arriagada, A., Recio-Blanco, A., de Laverny, P., et al. 2017, A&A, 601, A140
Salaris, M., Chieffi, A., & Straniero, O. 1993, ApJ, 414, 580
Salpeter, E. E. 1955, ApJ, 121, 161
Saracino, S., Dalessandro, E., Ferraro, F. R., et al. 2015, ApJ, 806, 152
Saracino, S., Dalessandro, E., Ferraro, F. R., et al. 2019, ApJ, 874, 86
Shibuya, T., Ouchi, M., Kubo, M., et al. 2016, ApJ, 821, 72
Sollima, A., Pancino, E., Ferraro, F. R., et al. 2005, ApJ, 634, 332
Stetson, P. B. 1987, PASP, 99, 191
Stetson, P. B. 1994, PASP, 106, 250
Tacchella, S., Carollo, C. M., Renzini, A., et al. 2015, Sci, 348, 314
Tolstoy, E., Hill, V., & Tosi, M. 2009, ARA&A, 47, 371
Tosi, M., Greggio, L., Marconi, G., et al. 1991, AJ, 102, 951
Ubeda, L., Anderson, J. & ACS Team 2012, AAS Meeting, 219, 241.03
van den Bergh, S., Abraham, R. G., Ellis, R. S., et al. 1996, AJ, 112, 359
Vasiliev, E., & Baumgardt, H. 2021, MNRAS, 505, 5978
Zinnecker, H., Keable, C. J., Dunlop, J. S., Cannon, R. D., & Griffiths, W. K. 1988, in IAU Symp. 126, The Harlow Shapley Symp. on Globular Cluster Systems in Galaxies, ed. J. E. Grindlay & A. G. Davis Philip (Dordrecht: Kluwer), 603